AIP Applied Physics Letters

Metal-interconnection-free integration of InGaN/GaN light emitting diodes with AlGaN/GaN high electron mobility transistors

Chao Liu, Yuefei Cai, Zhaojun Liu, Jun Ma, and Kei May Lau

Citation: Applied Physics Letters **106**, 181110 (2015); doi: 10.1063/1.4921049
View online: http://dx.doi.org/10.1063/1.4921049
View Table of Contents: http://scitation.aip.org/content/aip/journal/apl/106/18?ver=pdfcov
Published by the AIP Publishing

APPLIED PHYSICS LETTERS **106**, 181110 (2015)

Metal-interconnection-free integration of InGaN/GaN light emitting diodes with AlGaN/GaN high electron mobility transistors

Chao Liu,[a)] Yuefei Cai,[a)] Zhaojun Liu, Jun Ma, and Kei May Lau[b)]

Photonics Technology Center, Department of Electronic and Computer Engineering, Hong Kong University of Science and Technology, Clear Water Bay, Kowloon, Hong Kong

(Received 7 December 2014; accepted 30 April 2015; published online 8 May 2015)

We report a metal-interconnection-free integration scheme for InGaN/GaN light emitting diodes (LEDs) and AlGaN/GaN high electron mobility transistors (HEMTs) by combining selective epi removal (SER) and selective epitaxial growth (SEG) techniques. SER of HEMT epi was carried out first to expose the bottom unintentionally doped GaN buffer and the sidewall GaN channel. A LED structure was regrown in the SER region with the bottom n-type GaN layer (n-electrode of the LED) connected to the HEMTs laterally, enabling monolithic integration of the HEMTs and LEDs (HEMT-LED) without metal-interconnection. In addition to saving substrate real estate, minimal interface resistance between the regrown n-type GaN and the HEMT channel is a significant improvement over metal-interconnection. Furthermore, excellent off-state leakage characteristics of the driving transistor can also be guaranteed in such an integration scheme. © *2015 AIP Publishing LLC*. [http://dx.doi.org/10.1063/1.4921049]

InGaN/GaN light emitting diodes (LEDs) have attracted tremendous attention over the past decade due to their wide application in backlight units, automotive headlights, and general illumination. Meanwhile, GaN based field-effect transistors (FETs) are gaining ground in high power and high frequency switching applications because of advantages including high breakdown, high operating frequency, wide operating temperature range, and low power loss.[1–3] Sharing the same GaN-based material system, monolithic integration of HEMTs and LEDs can effectively reduce undesirable parasitic components and greatly improve the system stability as well as reliability. However, there are limited reports on the monolithic integration of the two kinds of devices, probably due to the significant difference in material requirements for LEDs and transistors as well as the complexity of device fabrication. Li *et al*.[4,5] and Lee *et al*.[6] demonstrated monolithic integration of GaN transistors with LEDs using a selective epi removal (SER) process with IC-type metal interconnections. Although seemingly feasible, the lack of control in the etch stop location and plasma damage to the exposed surface can lead to considerable transistor degradation. Recently, we reported an alternative approach: selective epitaxial growth (SEG) of AlGaN HEMTs on LEDs for HEMT-LED integration.[7,8] We demonstrated integrated HEMT-LED devices exhibiting comparable performance with respect to stand-alone HEMTs and LEDs. In this first experiment, there was difficulty in running reliable metal interconnects across the greatly enhanced epi growth at the interface region between the SEG epi and the SiO_2 mask.[9,10] The outputs of the HEMTs were therefore connected to the cathodes of the LEDs by wire-bonding. Furthermore, the metal wire interconnection may introduce extra parasitic components and degrade the performance of the integrated devices, especially for high frequency operation applications.

To minimize the parasitic issues, we introduce an integration scheme combining the SER and SEG methods to create a monolithically integrated HEMT-LED device without metal-interconnection. After growth of a HEMT structure, SER was performed to expose the bottom GaN buffer and the channel sidewall of the HEMT for the LED growth. To eliminate metal for better electrical connection, it is critical to achieve seamless contact between the GaN channel of the AlGaN/GaN HEMTs and the n-type GaN layer of the InGaN/GaN LEDs during the subsequent LED regrowth. A schematic of the finished HEMT-LED device can be found in Fig. 1. This integration scheme not only simplifies the device fabrication procedure but also eliminates parasitic components introduced by metal interconnects.

The AlGaN/GaN HEMT structure used in this work was grown on a 2 in. sapphire substrate in an Aixtron 2400HT metal organic chemical vapor deposition (MOCVD) reactor. Trimethylgallium (TMGa), trimethylaluminum (TMAl), and ammonia (NH_3) were used as Ga, Al, and N sources, respectively. Nitrogen and hydrogen were used as carrier gases. From bottom to top, the AlGaN/GaN HEMT structure was

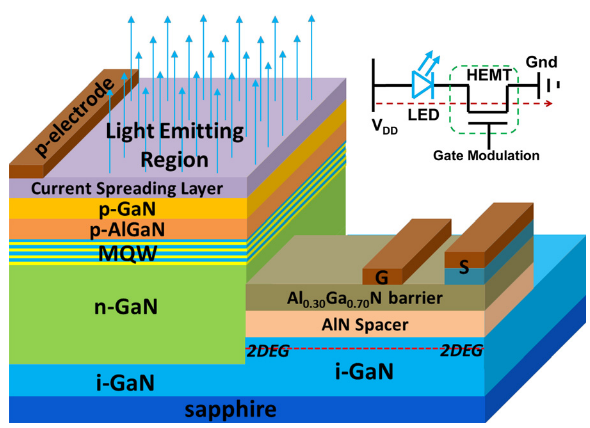

FIG. 1. Schematics of the finished HEMT-LED device. The inset shows the equivalent circuit diagram of the integrated HEMT-LED device.

a)C. Liu and Y. Cai contributed equally to this work.
b)Email: eekmlau@ust.hk. Tel.: (852)23587049. Fax: (852) 23581485.

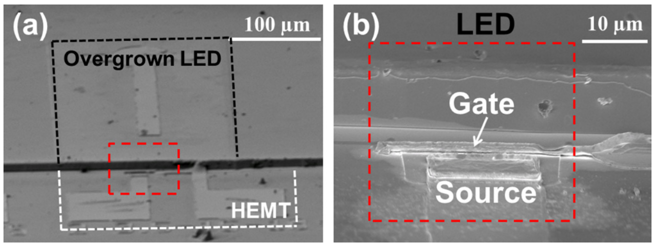

FIG. 2. 70° tilted SEM images of (a) the finished HEMT-LED device and (b) zoomed in image of the region near regrowth interface.

composed of a 3.0 μm GaN buffer, a 100 nm unintentionally doped GaN channel layer grown at a higher pressure and a higher V/III ratio for enhanced 2DEG mobility, a 1 nm AlN spacer layer, and a 20 nm $Al_{0.3}Ga_{0.7}N$ barrier layer. Hall effect measurement showed a sheet resistance of 330 $\Omega/\square$ with a Hall mobility of 1530 $cm^2/V\,s$ and a sheet carrier concentration of $1.2 \times 10^{13}\,cm^{-2}$. After the HEMT growth, a thin SiO_2 layer was deposited by plasma-enhanced chemical vapor deposition (PECVD) and patterned by buffered oxide etch (BOE). Inductively coupled plasma (ICP) etching was performed to selectively remove the AlGaN/AlN stack and expose the GaN buffer underneath. Afterwards, selective area growth of a standard GaN LED structure was carried out on the etched region. The overgrown LED epi started with a 1.6 μm n-type GaN, serving as the cathode of the LED and the drain of the HEMT. Subsequently, five periods of InGaN/GaN MQWs with 3 nm-thick wells and 11 nm-thick barriers were grown, followed by a 15 nm-thick p-$Al_{0.15}Ga_{0.85}N$ and a 170 nm p-type GaN layer.

Device fabrication started with definition of mesas for the LEDs (450 μm $\times$ 460 μm) by ICP etching, while the HEMT region was protected by photoresist. Then mesas of HEMTs were created with the LED area protected. Source ohmic contacts of the HEMTs were formed by e-beam evaporation of Ti/Al/Ni/Au and rapid thermal annealing (RTA) at 850 °C for 30 s in N_2 ambient. Afterwards, a Ni/Au current spreading layer and a Ti/Al/Ti/Au p-electrode of the LEDs were evaporated. Finally, Ni/Au gate metallization was realized for the HEMTs.

The surface morphology of the fabricated HEMT-LED device was characterized by scanning electron microscopy (SEM) at a 70° tilt angle. As shown in Fig. 2(a), the 2DEG channel of the HEMTs is in intimate contact with the n-type layer of the LEDs without additional metal, completing a three-terminal HEMT-LED device. The zoomed-in SEM image in Fig. 2(b) illustrates the gate and source electrodes of the HEMTs. A raised epi peak near the regrowth edge, due to the enhanced growth rates induced by loading effect, was an issue for metal coverage using the old metal interconnection. In the present design of connecting the HEMTs and the LEDs using the regrown n-type GaN, no such concern exists.

Atomic force microscopy (AFM) was carried out to investigate the surface morphology evolution in an area of $5 \times 5\,\mu m^2$. Fig. 3(a) presents the AFM image of the as-grown HEMT surface. The root mean square (RMS) roughness was 1.3 nm and well-aligned step flow patterns were observed, indicating a smooth surface. After the SER of 1.2 μm HEMT epi by ICP etching, the exposed GaN buffer exhibited a rougher surface with an RMS roughness value of 56.4 nm, as displayed in Fig. 3(b). Some triangular bumps with a height of around 400 nm remain on the GaN buffer, which might be caused by the un-optimized ICP etching conditions. The surface morphology of the overgrown LED sample is shown in Fig. 3(c). The RMS roughness was reduced to 0.9 nm after LED regrowth, accompanied by a step-flow surface morphology, indicating a smooth surface achieved after LED regrowth. The pits on the overgrown LED surface were due to the low growth temperature (980 °C) of the p-type GaN layer.

For integrated devices, interconnection related parasitic components play a vital role in the device performance, especially for high frequency applications. Figs. 4(a) and 4(b) compare the integration related resistances for the integration schemes used in previous work and this work, respectively. For all the integration schemes reported previously, the HEMTs and LEDs were connected through metal wires.[4–8] Metal-interconnect related resistances include the contact resistance between the metal and n-type layer of the LEDs (R_{c2}), metal wire resistance (R_{metal}), and the contact resistance between the metal and AlGaN barrier of the HEMTs (R_{c3}). Transmission-line modeling (TLM) measurements were used to extract the contact resistances. Measured R_{c2} and R_{c3} values were 0.47 Ω mm and 1.48 Ω mm, respectively, while R_{metal} was generally negligibly small in comparison. Using the metal-interconnection-free integration scheme shown in Fig. 4(b), the only interconnection resistance is the interface resistance (R_i) between the GaN channel of HEMTs and the n-type GaN of LEDs resulted after regrowth. Typically, R_i is in the range of 0.05–0.08 Ω mm,[11,12] which depends on the 2DEG concentration near the interface.[13] Therefore, the interconnection resistance was effectively reduced by one order of magnitude in the metal-interconnection-free integration scheme. The reduced parasitic resistance accounts for approximately 15% of the total parasitic resistance of the driving circuit, which can help cut down the delay time (RC) of the driving circuit. Besides the

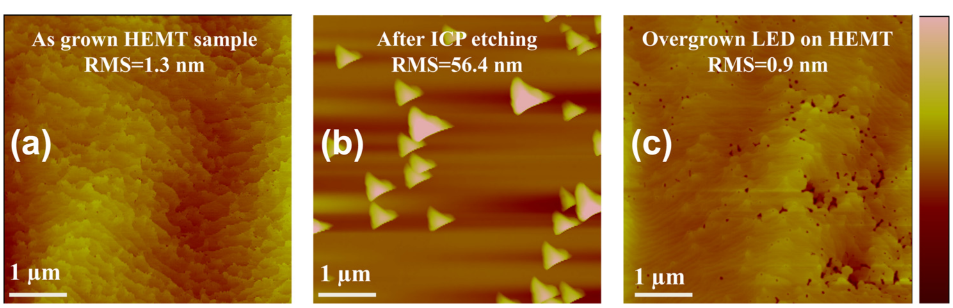

FIG. 3. Surface morphology of (a) as-grown HEMT-epi, (b) ICP exposed GaN buffer, and (c) overgrown LED sample, Vertical scale bar is 20 nm, 500 nm, and 20 nm for (a), (b), and (c), respectively.

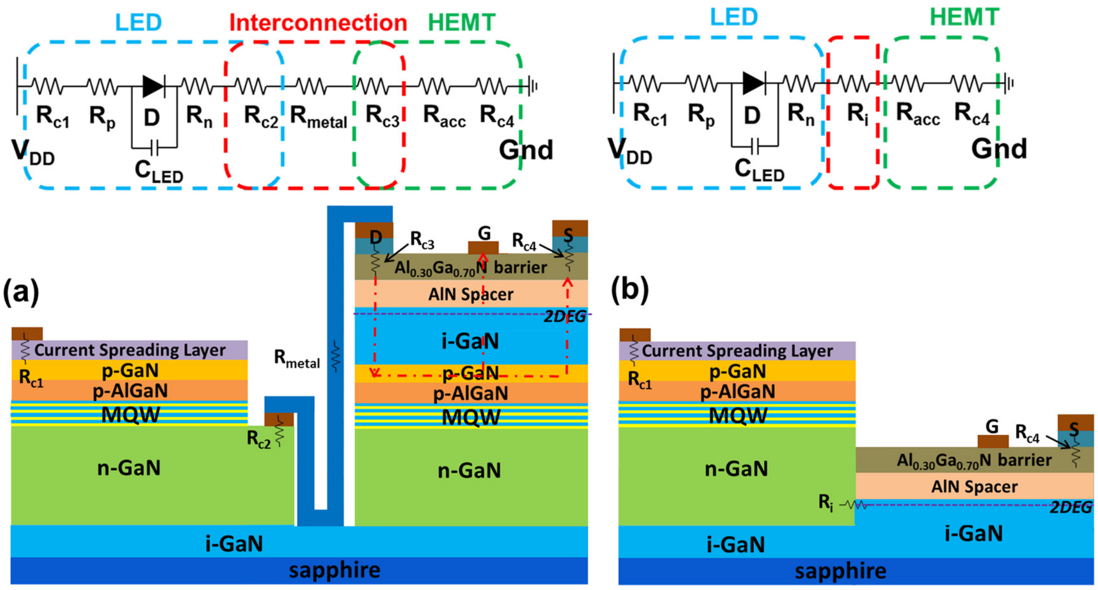

FIG. 4. Schematics of (a) the integration schemes used in previously reported works and (b) the metal-interconnection-free integration scheme reported in this work. The inset shows the equivalent circuit diagrams of the two kinds of integrated HEMT-LED devices.

delay consideration, inductance of the metal interconnects and voltage drop across the related parasitic resistances increase electrical power dissipation. This will result in lower luminous efficiency and higher heat generation, especially under high current injection condition. Furthermore, the metal-interconnection-free integration scheme can also lead to a smaller footprint, reduced fabrication complexity, and enhanced device reliability, compared to the integrated HEMT-LED via metal wire interconnects.

To highlight the advantage of growing LEDs after HEMTs over the stacked HEMTs on LEDs in our previous work, [7,8] we compare the off-state leakage characteristics of the HEMTs in Fig. 5(a). The drain-to-gate distance (L_{GD}) for the two kinds of HEMTs was both 15 μm. Using the former approach, the off-state leakage current density (I_{OFF}) of the HEMTs on LEDs rapidly increases to 1 mA/mm at a drain-to-source bias (V_{DS}) of 40.5 V. Such a poor leakage characteristic was attributed to the insufficient isolation from the underlying conductive p-type GaN layer in the LED structure, as shown in Fig. 4(a). In contrast, for the laterally connected LEDs with HEMTs in this work, the I_{OFF} of the HEMTs remains at a low level (around 3 orders lower) and only reaches 6.3 μA/mm at V_{DS} of 200 V, indicating a high buffer resistivity was retained after the high-temperature selective area growth process.

The output characteristics (I-V) of the discrete HEMTs and the integrated HEMT-LED devices are plotted in Fig. 5(b). The fabricated HEMTs have a gate length of 2 μm and a gate width of 100 μm with a gate to drain distance of 15 μm and a gate to source distance of 3.5 μm. The maximum output current density and the on-state resistance (R_{on}) of the discrete HEMT are around 420 mA/mm and 12.8 Ω mm, respectively. It is worth noting that there is minimal discrepancy between the I-V curves of the discrete HEMTs and the integrated HEMT-LED devices, except that the I-V curve of the integrated HEMT-LED device shifted towards positive voltage by around 3 V. This is caused by the LED device, serially connected to the driving HEMT, which requires a turn-on voltage to start a forward current flow at a low bias condition. At high bias conditions, the R_{on} of the LEDs (11 Ω) becomes negligible compared to that of the stand-alone HEMTs (128 Ω), and the driving current is no longer limited by the LED part. This explains the comparable R_{on} of the integrated HEMT-LED devices to that of the discrete HEMTs.

Fig. 6(a) presents the forward current and the light output power (LOP) of the HEMT-LED devices versus the applied gate bias of the integrated HEMTs, at three different V_{DD}. To reduce the power dissipation and heat generation from the driving transistor and improve current spreading

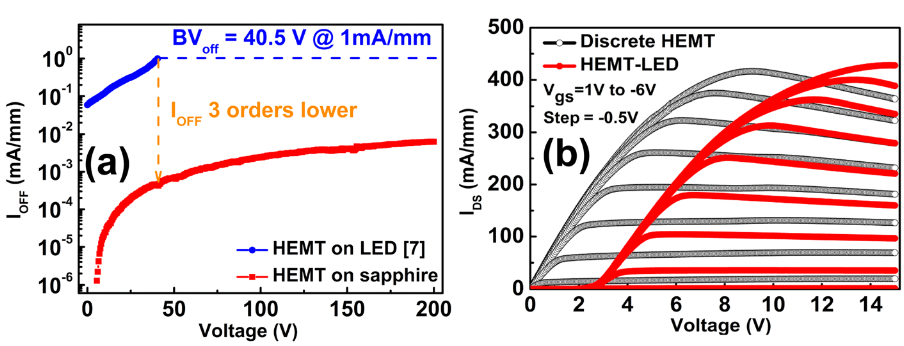

FIG. 5. (a) Off-state leakage characteristics of the discrete HEMTs on LEDs and sapphire and (b) output characteristics of the discrete HEMT and integrated HEMT-LED device, respectively.

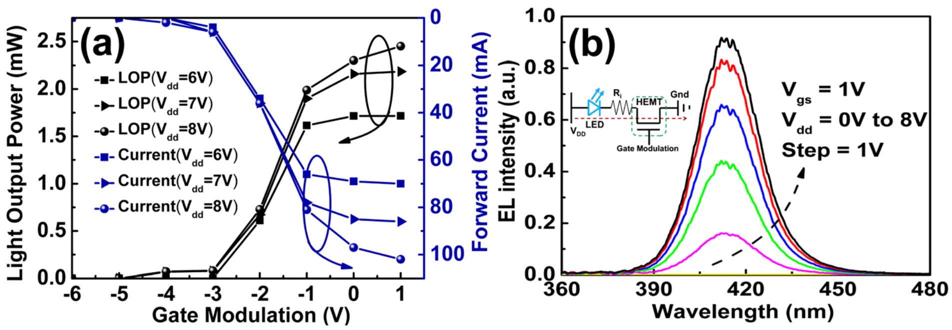

FIG. 6. (a) Light output power and I-V characteristics of the fabricated HEMT-LED device modulated by gate biases at different drain voltages and (b) EL spectrum modulated by V_{DD} at $V_{GS} = 1$ V.

from the driving HEMTs to the LEDs, a HEMT with a larger W_g/L_g (475 μm/2 μm) was used in the integrated HEMT-LED devices. The forward current of the HEMT-LED devices can be well controlled by the gate bias of the driving transistor. In addition, the LOP of the integrated LEDs exhibits the same response as the driving current of the integrated HEMTs, demonstrating good controllability of the LEDs by the gate voltage via the injected current. Besides the gate modulation capability, light emission of the integrated LED can also be suitably controlled by the V_{DD} of the HEMT-LED device. Fig. 6(b) shows the electroluminescence (EL) spectrum from the integrated HEMT-LED device at a fixed gate bias of 1 V with changing V_{DD} from 0 to 8 V at 1 V steps.

In conclusion, we have demonstrated a metal-interconnection-free HEMT-LED device using a SEG process, enabling direct contact between the GaN channel of HEMTs and the n-electrode of LEDs. In addition to exhibiting good characteristics in the modulation of LED brightness by the driving transistor through gate control of the injected driving current, this monolithic integration scheme warrants excellent off-state characteristics of the driving transistor and minimized parasitic components. We believe the demonstrated integration scheme of the HEMT-LED is highly promising for a wide range of applications, such as smart lighting, displays, and optical communications.

This work was supported in part by Grants (614312 and T23-612/12-R) from the Research Grants Council of Hong Kong. The authors gratefully thank Qiang Li, Xing Lu, Tongde Huang, Xinbo Zou, and Bei Shi for their many helpful discussions, and Wilson Tang as well as the staff of the MCPF and NFF of HKUST for their technical support.

[1] K. Joshin, T. Kikkawa, S. Masuda, and K. Watanabe, Fujitsu Sci. Tech. J. **50**, 138 (2014), available at http://www.fujitsu.com/downloads/MAG/vol50-1/paper21.pdf.
[2] J. W. Chung, W. E. Hoke, E. M. Chumbes, and T. Palacios, IEEE Electron Device Lett. **31**, 195 (2010).
[3] P. Herfurth, D. Maier, L. Lugani, J. F. Carlin, R. Roesch, Y. Men, N. Grandjean, and E. Kohn, IEEE Electron Device Lett. **34**, 496 (2013).
[4] Z. Li, J. Waldron, T. Detchprohm, C. Wetzel, R. F. Karlicek, Jr., and T. P. Chow, Appl. Phys. Lett. **102**, 192107-1 (2013).
[5] Z. Li, J. Waldron, S. Chowdhury, L. Zhao, T. Detchprohm, C. Wetzel, R. F. Karlicek, Jr., and T. P. Chow, "High temperature characteristics of monolithically integrated LED and MOS-channel HEMT in GaN using selective epi removal," Phys. Status Solidi A (published online).
[6] Y. Lee, Z. Yang, P. Chen, Y. Hsieh, Y. Yao, M. Liao, M. Lee, M. Wang, and J. Hwang, Opt. Express **22**, A1589 (2014).
[7] Z. Liu, T. Huang, J. Ma, C. Liu, and K. M. Lau, IEEE Electron Device Lett. **35**, 330 (2014).
[8] Z. Liu, J. Ma, T. Huang, C. Liu, and K. M. Lau, Appl. Phys. Lett. **104**, 091103-1 (2014).
[9] G. Brammertz, Y. Mols, S. Degroote, M. Leys, J. V. Steenbergen, G. Borghs, and M. Gaymax, J. Cryst. Growth. **297**, 204 (2006).
[10] A. Ishitani, N. Endo, and H. Tsuya, Jpn. J. Appl. Phys. **23**, L391 (1984).
[11] T. D. Huang, Z. J. Liu, X. L. Zhu, J. Ma, and K. M. Lau, IEEE Trans Electron. Devices **60**, 3019 (2013).
[12] J. Guo, G. Li, F. Faria, Y. Cao, R. Wang, J. Verma, X. Gao, S. Guo, E. Beam, A. Ketterson, M. Schuette, P. Saunier, M. Wistey, D. Jena, and H. Xing, IEEE Electron Device Lett. **33**, 525 (2012).
[13] P. M. Solomon, A. Palevski, T. F. Kuech, and M. A. Tischler, *International Technical Digest on Electron Devices Meeting* (IEEE, 1989), pp. 405.